Geomorphology 129 (2011) 190–203

Contents lists available at ScienceDirect

Geomorphology

journal homepage: www.elsevier.com/locate/geomorph

Comparison of four methods to calculate aeolian sediment transport threshold from field data: Implications for transport prediction and discussion of method evolution

Thomas E. Barchyn *, Chris H. Hugenholtz

Department of Geography, University of Lethbridge, 4401 University Drive, Lethbridge, Alberta, Canada, T1K 3M4

ARTICLE INFO

Article history:
Received 24 June 2010
Received in revised form 26 January 2011
Accepted 28 January 2011
Available online 4 February 2011

Keywords:
Aeolian sediment transport
Threshold
Measurement
Methods

ABSTRACT

Aeolian sediment transport threshold is commonly defined as the minimum wind speed (or shear stress) required for wind-driven sediment transport. Accurate and consistent quantification of this threshold is essential because it is an input variable in models used to predict wind erosion, dune activity, and dust emissions. The majority of threshold quantification has been performed with analogs (analytical models or wind tunnels); however, in the past few decades field-based approaches to threshold parameterization have become more common. Although several methods of calculating transport threshold from field data are available, their comparability is unknown. To address this issue we collected high resolution sediment transport and wind measurements (1 Hz) on an active sand dune for 11 days and compared four different methods of calculating threshold: (i) time fraction equivalence method (TFEM); (ii) Gaussian time fraction equivalence method (GTFEM); (iii) instantaneous method; and (iv) regression method. Time-paired measurements from the two most widely used methods (TFEM and GTFEM) were strongly correlated ($r=0.977$); however, correlations between other methods varied (from $r=0.861$ to $r=0.261$). To demonstrate the implications of using different threshold calculation methods we predicted mass transport, which ranged from 63.6 (instantaneous method) to 126.6 kg per crosswind meter (regression method). This inconsistency suggests that the threshold calculation method could have an appreciable impact on transport predictions. Threshold values are similarly inconsistent when the measurement interval is modified. As such, we do not recommend comparing any measured threshold with another. We discuss several strategies that may mitigate the impact of this issue such as clarification of semantics and method standardization. We also discuss several criticisms of field-based threshold measurements and re-conceptualizations that could allow investigators to develop a better understanding of field-based measurements. Overall, results from this study could allow future investigators to improve threshold (and transport) predictions.

© 2011 Elsevier B.V. All rights reserved.

1. Introduction

Aeolian sediment transport threshold (subsequently referred to as 'threshold') is commonly defined as the minimum wind speed (or shear stress) required for wind-driven sediment transport. A variety of surface controls modify threshold such as moisture (e.g., Ravi and D'Odorico, 2005), vegetation (e.g., Wolfe and Nickling, 1993), biogenic crusts (e.g., Argaman et al., 2006), slope (Howard, 1977), and pore ice (e.g., McKenna Neuman, 1990).

Threshold measurements have several important applications. Threshold is a central parameter in most models predicting sediment transport (e.g., Lettau and Lettau, 1978), wind erosion (e.g., Fryrear et al., 2000), dune activity (e.g., Lancaster and Helm, 2000), and dust emissions (e.g., Marticorena and Bergametti, 1995). When wind speed varies near threshold, model predictions are highly sensitive to the value(s) used (Arens, 1996). Threshold also has practical applications as a standalone parameter. For example, Stout and Arimoto (2010) used threshold to track the temporal patterns in aeolian transport of radionuclide contaminated soil. De Oro and Buschiazzo (2009) used threshold to explore seasonal changes in the susceptibility of an agricultural field to wind erosion.

There have been a variety of methods developed to parameterize thresholds, including: (i) analytical models (e.g., Bagnold, 1941), (ii) wind tunnels (e.g., Nickling, 1988), (iii) air guns (e.g., Li et al., 2010) and (iv) field measurements (e.g., Stout, 2004). Although parameterizations from (i), (ii) and (iii) are invaluable from experimental and theoretical standpoints, these parameterizations can be challenging to apply. In cases, successful application is limited by the investigators' ability to measure or predict surface conditions (see examples of difficulties with measuring surface moisture: Ravi and D'Odorico, 2005; Darke and McKenna Neuman, 2008; Delgado-Fernandez et al., 2009; Nield et al., 2011). In addition, turbulence and sediment transport characteristics in some analogs have been noted to be different from those observed in the field (e.g., wind tunnels: Farrell and Sherman, 2006;

* Corresponding author. Tel.: +1 403 332 4043; fax: +1 403 332 4039.
E-mail address: tom.barchyn@uleth.ca (T.E. Barchyn).

0169-555X/$ – see front matter © 2011 Elsevier B.V. All rights reserved.
doi:10.1016/j.geomorph.2011.01.022

Sherman and Farrell, 2008). Consequently, many investigators have turned to field-based measurement to develop (potentially) more reliable measurements.

We first describe the general approach for measuring threshold in the field. Most methods are based on high resolution (≈1 Hz) time series of wind speed and sediment transport. These data are collected with computerized data logging systems, fast responding anemometers, and electronic sediment transport sensors (e.g., Stockton and Gillette, 1990; Spaan and van den Abeele, 1991; Baas, 2004). From these high resolution records of transport and wind speed, thresholds are typically calculated in discrete temporal intervals with several methods (e.g., Stout and Zobeck, 1996; Stout, 2004; Schönfeldt, 2004). In most methods there are two time intervals that require specification: (i) *sampling interval*: the rate that raw data are collected (typically 1 Hz); and (ii) *measurement interval*: the rate that threshold measurements are calculated (typically minutes).

In the past several decades the use of field-based threshold measurement systems has increased (see Table 1 for summary of methods in recent studies). Many studies have found that threshold dynamics are pervasive and poorly understood, especially in semi-arid or coastal environments (e.g., Arens, 1996; Davidson-Arnott et al., 2005; Wiggs et al., 2004b; Davidson-Arnott and Bauer, 2009; Sankey et al., 2009a, 2009b).

Parallel to progress in measuring field-based threshold, many investigators have closely examined the methods used. Stout (1998) examined the impact of modifying sampling interval. Wiggs et al. (2004a) furthered this research and examined the impact of modifying both sampling and measurement intervals. Baas (2004), Van Pelt et al. (2009), and Barchyn and Hugenholtz (2010) compared electronic sediment transport sensors and found inconsistencies in response between manufacturers, sensors, and around the circumference of individual sensors. In general, most work has found that modifying the aspects of the measurement system can affect the threshold values produced. A lack of consistency in methods (see Table 1) suggests that there are a variety of individual definitions of the measurement of 'threshold', and the results from one study may be difficult to reliably compare with another. This could pose a challenge for developing reliable transport models that use synthesized data from numerous environments.

In this study, we further previous research by examining the impact of modifying the calculation method. We collected high resolution wind and sediment transport data (1 Hz) on an active sand

Table 1
Summary of methods used by recent studies employing field-based threshold measurement methods. N/A = information not provided in study.

Study	Calculation method	Sampling interval	Measurement interval	Sediment transport sensor			Anemometer	
				Type[a]	Height (mm)	Area (mm^2)	Type (distance constant)	Height (m)
This study	Various	1 Hz	Various	Sensit H11-B	50	337.5	RM Young 5103 (2.7 m)	1.35
Arens, 1996	Regression	0.2 Hz	1–42 h.	Saltiphone	100	201.0[b]	N/A	5.0
Barchyn and Hugenholtz, 2010	Instantaneous	1 Hz	N/A	Sensit H11-B	50	337.5	RM Young 5103 (2.7 m)	1.35
Davidson-Arnott et al.,2005	TFEM, u_{tmin}, u_{tmax}[c]	1 Hz (0.2 Hz)[d]	18–25 min	Balance trap	0–500	5000	RM Young cup, (2.3 m)	0.3
Davidson-Arnott et al., 2008	TFEM, u_{tmin}, u_{tmax}[c]	1 Hz	10 min	Safire	20	323.0[e]	RM Young cup, DC (2.3 m)	0.3
Davidson-Arnott and Bauer, 2009	TFEM, $u_{t\ min}$, $u_{t\ max}$[c]	1 Hz	10 min	Safire	20	323.0 [e]	RM Young cup, DC (N/A)	0.6
De Oro and Buschiazzo, 2009	GTFEM	1 Hz (sediment) 1 min (wind)	5 min	Sensit	20	337.5 [e]	N/A	2.0
Gillette et al., 1997b	Regression	20 min	N/A	Sensit	100	337.5 [e]	MetOne 014	2.0
Larney et al., 1995	$u_{t\ min}$ [c]	2 min	2 min	Sensit	50	337.5 [e]	N/A	2.0
McKenna Neuman et al., 2000	TFEM	10 s	16–120 min	Balance trap	N/A	N/A	RM Young cup (2.8 m)	0.3
Ravi and D'Odorico, 2005	N/A	1 Hz [e]	5 min [f]	Sensit H7	N/A	337.5 [e]	RM Young 5103 [f] (2.7 m) [g]	3.0
Sankey et al., 2009a, 2009b	GTFEM	1 Hz	5 min	Sensit	50	337.5 [e]	MetOne 014A (4.5 m) [h]	2.0
Schönfeldt, 2004	TFEM, regression	1 Hz	5 min	Saltiphone	35	201.0 [b]	Gill cup (N/A)	0.35
Speirs et al., 2008	GTFEM	8 Hz	1 min	Sensit	N/A	337.5 [e]	Cup (N/A)	2.1
Stout, 2004	GTFEM	1 Hz	5 min	Sensit	50	337.5 [e]	RM Young 5103 [i] (2.7 m) [g]	2.0
Stout, 2007	GTFEM	1 Hz	5 min	Sensit	50	337.5 [e]	RM Young 5103 [j] (2.7 m) [g]	2.0
Stout and Arimoto, 2010	GTFEM	1 Hz	5 min	Sensit	N/A	337.5 [e]	N/A	2.0
Stout and Zobeck, 1997	TFEM	1 Hz	5 min	Sensit	0	337.5 [e]	cup (2.3 m)	2.0
Stout and Zobeck, 1996	TFEM	1 Hz	3 min	Sensit	0	337.5 [e]	cup (N/A)	2.0
Udo et al., 2008	TFEM	1 Hz	5 min	UD-101; Sensit	40	113 (UD-101)	Delta Ohm (sonic) (0) [k]	0.9
Wiggs et al., 2004a	TFEM	1–60 s	20 min	Sensit H7	0	337.5 [e]	Flow master (thermal) (0) [k]	0.25; 0.1
Wiggs and Holmes, in press	TFEM	1 min	13–16 days	Safire (version 1.5)	0	323.0 [e]	Vector A-100R (2.3 m)[m]	2.3
Zobeck and Van Pelt, 2006	GTFEM	1 Hz	1 min	Sensit	0	337.5 [e]	cup (N/A)	2.0

[a] References for further information on each sediment transport sensor are as follows: Sensit (Stockton and Gillette, 1990; Stout and Zobeck, 1997; Van Pelt et al., 2009); Safire (Baas, 2004; Van Pelt et al., 2009); Balance trap (Davidson-Arnott et al., 2005; Nickling and McKenna Neuman, 1997); UD-101 (Udo, 2009); Saltiphone (Spaan and van den Abeele, 1991; Van Pelt et al., 2009).

[b] We assume that the Saltiphone used is identical dimensions to that of the sensor described in Spaan and Van den Abeele (1991).

[c] $u_{t\ min}$ is a threshold measurement method that is equal to the minimum wind speed with saltation; $u_{t\ max}$ is a threshold measurement method that is equal to the maximum wind speed without saltation; both methods are described by Davidson-Arnott et al. (2005). Various averaging schemes have been developed, refer to original sources for analysis details.

[d] Sediment transport and wind speed data were smoothed with a running 5 s mean filter.

[e] Sediment transport sensor dimensions are assumed to be identical to those measured in Barchyn and Hugenholtz (2010).

[f] We assumed these data are from United States Geological Survey CLIM-MET internet site; instrument parameters are described here: http://esp.cr.usgs.gov/info/sw/clim-met/anatomy/index.html (accessed: 03 October 2010).

[g] RM Young 5103 anemometer distance constants are assumed to be identical to current specifications as published at: http://www.campbellsci.com/documents/manuals/05103.pdf (accessed: 03 October 2010).

[h] MetOne 014A anemometer distance constant is assumed to be identical to current specifications as published at: http://www.campbellsci.com/documents/manuals/014a.pdf (accessed: 03 October 2010).

[i] Anemometer model was determined from a photo (Fig. 5) in Stout (2004).

[j] Anemometer model was determined from a photo (Fig. 3) in Stout (2007).

[k] Sonic and thermal anemometers are assumed to have negligible inertia, and consequently have been assigned a distance constant of zero.

[m] Distance constant was not published, the distance constant for this type of anemometer is assumed to be identical to that published here: http://www.windspeed.co.uk/ws/index.php?option=displaypage&op=page&Itemid=67 (accessed 09 December 2010).

dune for 11 days. These field data were used as input in four different threshold calculation methods: (i) time fraction equivalence method (TFEM; Stout and Zobeck, 1996, 1997), (ii) Gaussian time fraction equivalence method (GTFEM; Stout, 2004), (iii) instantaneous threshold (Barchyn and Hugenholtz, 2010; also discussed by Schönfeldt, 2004), and (iv) regression threshold (Gillette et al., 1997b; Schönfeldt, 2004). We also investigate how the use of different threshold calculation methods can affect prediction of mass flux and examine the impact of modifying measurement interval on each calculation method. Overall, results reveal inconsistency among the four methods that can modify mass transport predictions. In an extended discussion, we explore the impact of these findings and examine several strategies that could increase the reliability and comparability of field-based measurements of threshold.

2. Field study and data collection

The purpose of the field study was to collect raw data, from which the four different methods of calculating threshold could be compared. This contrasts with typical threshold monitoring campaigns where the chosen method is pre-determined and programmed into the data logging system. The instrument array was designed to mimic instrument arrays used by other investigators (see Table 1), thus providing more realistic assessments.

2.1. Study area

Instruments were deployed on an active sand dune in the Bigstick Sand Hills of Saskatchewan, Canada (50° 12′ 31.55″ N, 109° 12′ 23.85″ W) (see Fig. 1). The Bigstick Sand Hills are approximately 360 km^2 in area. Sediment in the dunefield is derived from glaciofluvial and glaciolacustrine outwash deposited during the retreat of the Laurentide Ice Sheet (Klassen, 1994; Dyke and Prest, 1987; Wolfe et al., 2004). Dunes in the area have undergone several periods of activity and stabilization over the past 10000 years (Wolfe et al., 2001; 2006). Within the past two centuries dune activity has dramatically declined; presently only a handful of parabolic dunes and blowouts are active (Hugenholtz and Wolfe, 2005; Hugenholtz

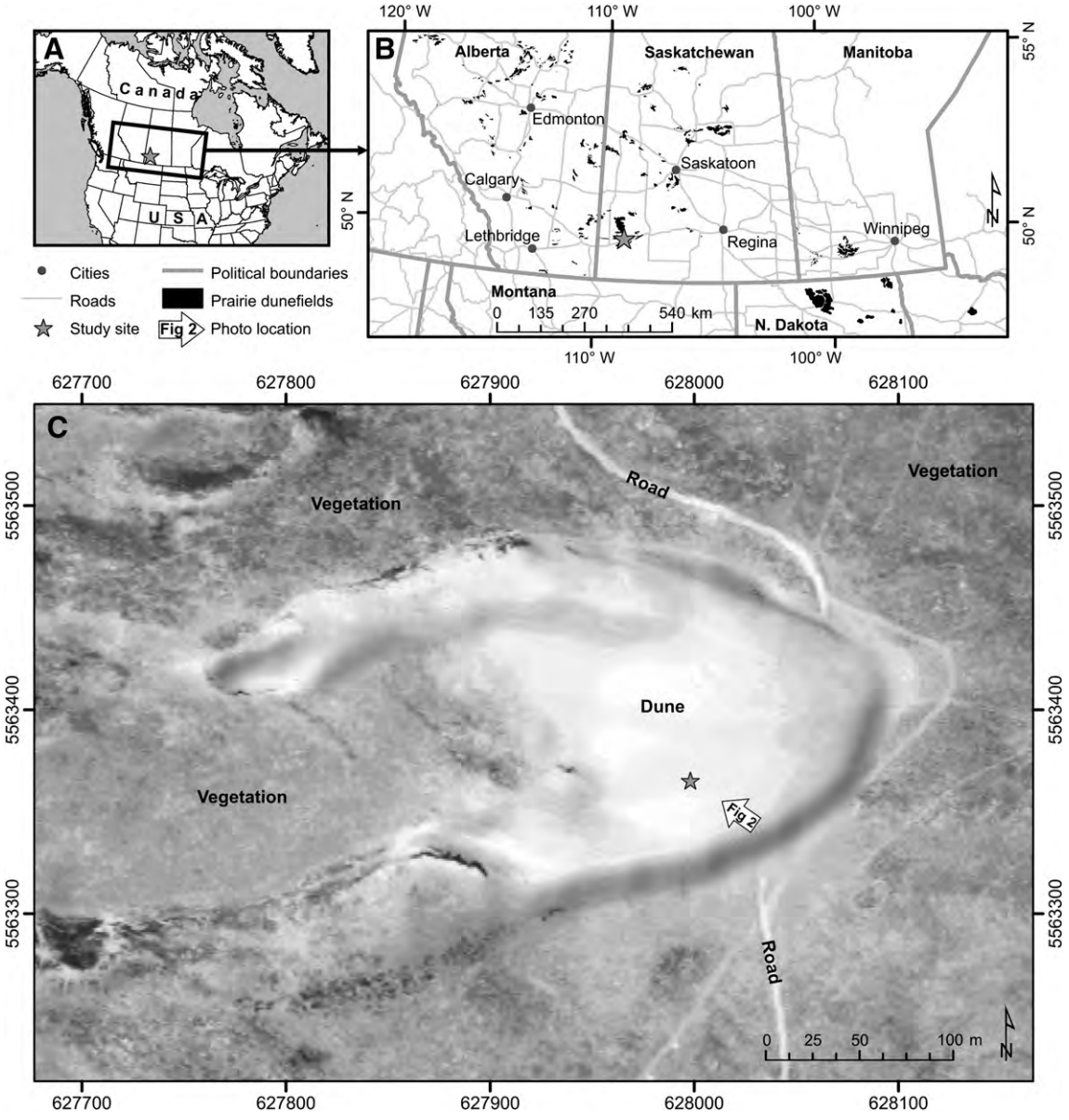

Fig. 1. Location of study area within A) North America, B) Northern Great Plains and C) on the sand dune. The location and direction of the photograph in Fig. 2 is shown on (C). Coordinates: C) UTM Zone 12 N.

et al., 2009). The present climate is continental with low precipitation, cold winters, and short, warm summers (classified as sub-humid to semi-arid). Average monthly temperatures range from −11 °C (January) to 19 °C (July). Annual precipitation averages 380 mm (110 mm as snow) (climate data from Hugenholtz et al., 2009).

The instrument array was deployed on the stoss slope of a parabolic dune (see Figs. 1 and 2). Two surface samples were collected on 14 July 2009 and 21 July 2009 to determine sediment grainsize. Samples were air dried and dry sieved. The graphic mean was 1.55 Φ, graphic standard deviation was 1.31 Φ. Ahlbrandt (1979) compiled the grain size data for 191 samples worldwide and derived an average graphic mean of 1.83 Φ, graphic standard deviation of 0.73 Φ. The sand on this dune is slightly coarser and less well sorted than typical dune sand, but is not anomalous for aeolian environments (Ahlbrandt, 1979). Further information on the characteristics of this specific dune can be found in Hugenholtz et al. (2009).

2.2. Data collection methods

The instrument array was deployed from 09 July 2009 to 21 July 2009 (see Fig. 2). Instruments measured data at 1 Hz continuously. The lengthy 11-day deployment increased the possibility of encountering a variety of threshold conditions. Instruments included a datalogger (Campbell Scientific CR1000), propeller anemometer and wind direction sensor (RM Young 5103, distance constant: 2.7 m, resolution at 1 Hz: 0.098 m s^{-1}, mounted at 1.35 m height), and a piezoelectric impact sensor (Sensit H11-B, mounted with the center of the piezoelectric element at 50 mm height and adjusted mid-deployment on 14 July 2009). Details on the performance of this Sensit H11-B in this specific deployment are available in Barchyn and Hugenholtz (2010). A time-lapse camera, co-located with the sensors, acquired images of the array every 0.5 h from 0600 to 2100 h daily. The images were used to ensure that the sensor was situated within 40–60 mm of the bed and to discern occurrences of rain-splashed sediment from wind-blown sediment. The datalogger was programmed to record data when a minimum of one count was recorded by the sensor in the previous 300 s and when a wind direction measurement was recorded between 225 and 330° during the previous 300 s. This conserved datalogger memory and ensured recorded sediment transport was not influenced by adjacent sensors. To avoid calculating threshold with erroneous data from rain drop impacts, we removed data when rain was present in images and/or recorded at a weather station located 2.65 km to the southeast. The site was enclosed with a fence for the entire deployment to prevent instrument damage from cattle.

3. Threshold calculation methods

From a review of the literature we selected four different methods of calculating aeolian sediment transport threshold. Comparisons were made among the methods in two manners: (i) with a constant measurement interval, and (ii) with a series of measurement intervals.

Comparisons made with a fixed measurement interval used a measurement interval of 5 min (the most common interval used in other investigations, Table 1). Raw data were used to calculate threshold at 5 min intervals from an origin of 17:15:00 on 09 July 2009. Thresholds were only calculated for measurement intervals with a complete record (300 s) of data. Comparisons were only performed for records when threshold could be calculated with all methods. In addition to comparing threshold values, mass transport predictions were made and compared.

For comparisons made with a differing measurement interval, we calculated a series of thresholds for the full dataset with measurement intervals ranging from 20 to 3600 s, in increments of 20 s. For each measurement interval, threshold was calculated for a sequence of measurement intervals following the origin (e.g., if measurement interval = 20 s, time intervals = 17:15:00, 17:15:20, 17:15:40, 17:16:00, etc.). Thresholds were only calculated if a complete record of data were present in the measurement interval and comparisons were only performed for measurement intervals when thresholds could be calculated with all methods. Contrary to Stout (1998) and Wiggs et al. (2004a), we retained a sampling (or 'averaging') interval of 1 Hz for these tests. All analyses were programmed in R, version 2.10.1, default parameters for functions were used unless otherwise noted (R Development Core Team, 2009).

We describe the mathematics of the methods below. Figs. 3 and 4 illustrate the general principles and generalizations behind each of the methods with a sample measurement interval selected at random from the deployment.

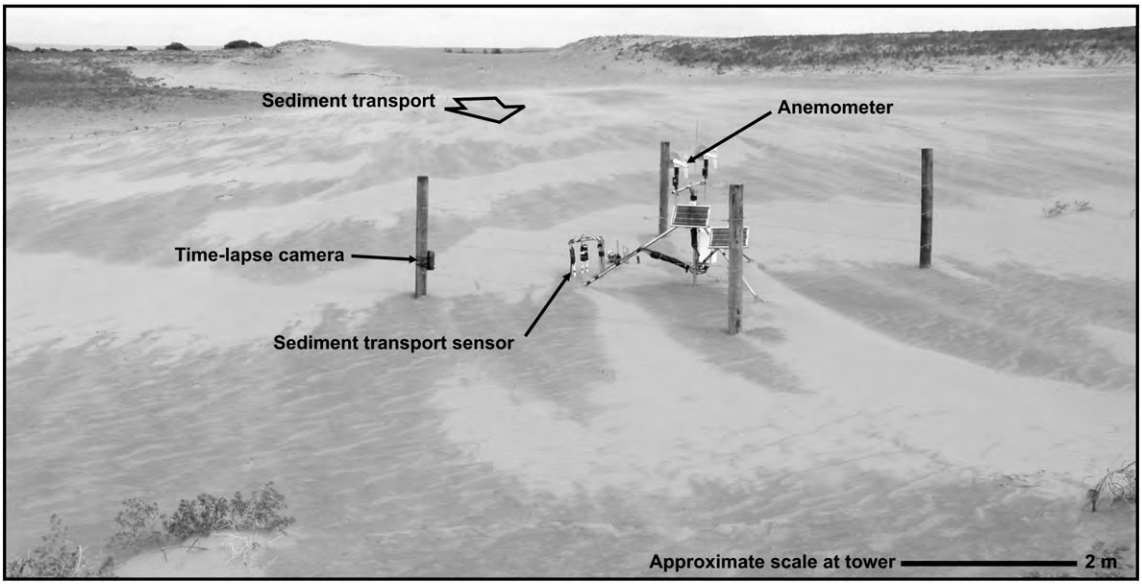

Fig. 2. Photograph of study site, looking upwind mid-deployment. Note spatial differentiation in dune surface moisture which could be responsible for a portion of measured threshold variability. The location of this photograph is marked on Fig. 1C.

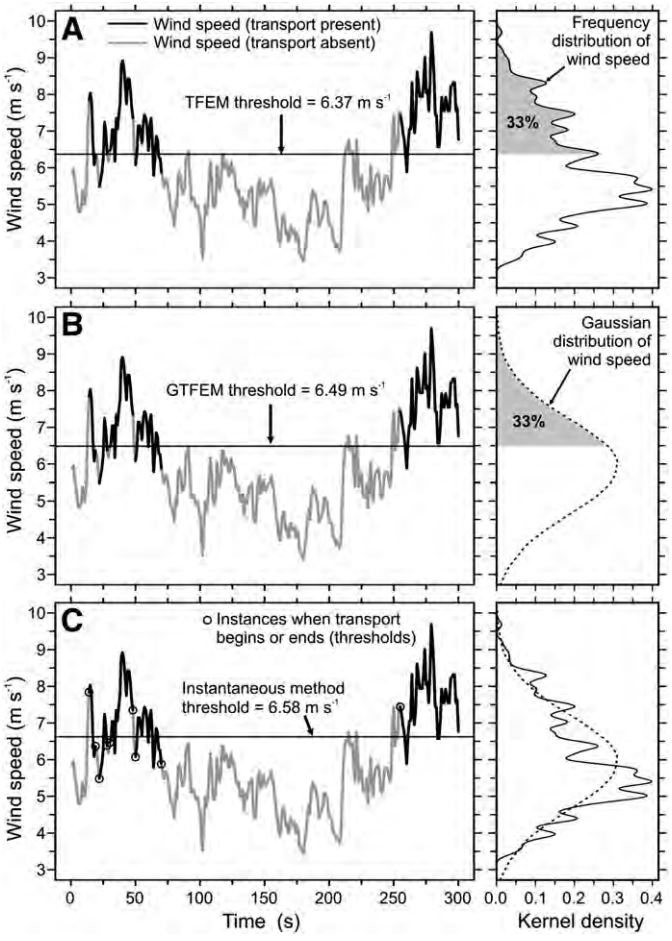

Fig. 3. Illustration of principles underlying threshold calculation methods for a sample measurement interval (wind speed mean = 5.92 m s^{-1}, standard deviation = 1.28 m s^{-1}, transport duration = 99 s. or 33% of 300 s.). A) Time fraction equivalence method. The frequency distribution of wind speeds represented by kernel density estimate (Kernel: Gaussian with standard deviation 0.1 m s^{-1}). The time fraction of the highest wind speeds is set to be equivalent to the time fraction of sediment transport. B) Gaussian time fraction equivalence method. The time fraction of the highest wind speeds in a Gaussian distribution is set to be equivalent to the time fraction of sediment transport. C) Instantaneous method: instances of transport beginning or ending are extracted (denoted by circles). The mean of all instantaneous thresholds for the measurement interval is recorded. All thresholds are marked for comparison in Fig. 4. Wind speeds measured at 1.35 m height.

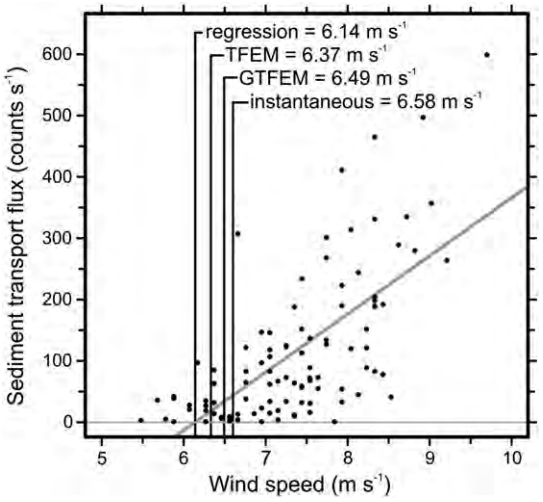

Fig. 4. Regression method for calculating threshold. A linear regression of non-zero measurements of sediment transport is performed, the intercept where sediment transport equals zero is the regression threshold. All thresholds from Fig. 3 are marked for comparison. Wind speeds measured at 1.35 m height.

3.1. Time fraction equivalence method

The time fraction equivalence method (TFEM, $u_{t\ TFEM}$) was introduced by Stout and Zobeck (1996, 1997) and subsequently reviewed by Wiggs et al. (2004a). With the TFEM, investigators assume that threshold can be represented by one wind speed (within a measurement interval), where sediment transport only occurs when wind speed is above threshold — and contrarily, no transport occurs when wind speed is below threshold. Within the measurement interval, the time fraction of wind speeds above threshold is set to be equivalent to the time fraction of sediment transport (see Fig. 3A).

We calculated the TFEM threshold with the following procedure, which is mathematically similar to the 'modified time fraction equivalence method' interpretation of Wiggs et al. (2004a). First, the total number of seconds of sediment transport was tabulated for each measurement interval. One second of sediment transport was recorded for each second when counts from the sediment transport were not zero. The number of wind speed measurements above threshold was determined by the number of seconds of sediment transport. Likewise, the number of wind speed measurements below threshold was determined by the number of seconds with no sediment transport. To ensure time fraction equivalence, the threshold must be between two wind speed measurements. For measurement intervals when sediment transport occurred intermittently $u_{t\ TFEM}$ is defined as:

$$u_{t\ TFEM} = \left(u_j + u_{j+1}\right)/2 \tag{1}$$

where $u_{t\ TFEM}$ is the TFEM threshold, j is the number of seconds sediment transport occurred, u_j is the *jth* wind speed measurement (ordered descending), likewise, u_{j+1} is the *(j+1)th* wind speed measurement (ordered descending) (Stout and Zobeck, 1996; 1997; Wiggs et al., 2004a). This method produces results identical to those produced by an iterative technique proposed by Stout and Zobeck (1996; 1997) in a manner that is more computationally efficient. Following Eq. (1), the resolution of the TFEM in this deployment is equivalent to half the resolution of the anemometer, calculated as 0.049 m s^{-1} at 1 Hz.

3.2. Gaussian time fraction equivalence method

The Gaussian time fraction equivalence method (GTFEM; $u_{t\ GTFEM}$) was developed by Stout (2004). The GTFEM method is similar to the TFEM method with an important modification. Instead of using measured wind speed values directly, the mean and standard deviation of wind speeds are calculated to synthetically reproduce the wind speed distribution as Gaussian (found to be the best synthetic distribution by Stout and Zobeck, 1997). Consequently, this method relies upon the assumption that wind speeds in the measurement interval closely follow a Gaussian distribution. The calculation of threshold remains similar; the fraction of time that sediment transport occurred is used to determine the fraction of wind speeds above threshold (see Fig. 3B). The GTFEM threshold is calculated as:

$$u_{t\ GTFEM} = \bar{u} - \sigma\,\Phi^{-1}(j/M) \tag{2}$$

where $u_{t\ GTFEM}$ is the GTFEM threshold, $\bar{u}$ is the mean wind speed in the measurement interval, σ is the standard deviation of wind speed,

Φ^{-1} (j/M) is the inverse normal distribution function of j (number of seconds sediment transport occurred) divided by M (the total number of seconds in the measurement interval). Other investigators have referred to j/M as 'intermittency', 'γ', or 'saltation activity'. As in Stout (2004), we removed measurements where j/M was less than 0.02 or higher than 0.98 because these calculations lie in the tails of the Gaussian distribution and are systematically unreliable. The advantage of this method is simple programming and efficient usage of datalogger memory; only the wind speed mean, standard deviation, and the number of seconds sediment transport occurred are required to be recorded for each measurement interval. The GTFEM threshold can be calculated easily post-deployment in a spreadsheet with a series of data manipulations.

3.3. Instantaneous method

The instantaneous method is a field interpretation of the traditional definition of threshold proposed by Bagnold (1941) (the minimum wind speed to initiate transport) (used by Barchyn and Hugenholtz, 2010; mentioned by Schönfeldt, 2004). The method identifies the wind speed when sediment transport begins or ends; these wind speeds correspond to the instances that threshold is passed (see Fig. 3C). We used the following rules to define wind speeds extracted as threshold measurements for each second in the time series:

$$\begin{array}{l} u_{t\ inst(i)} = u_i \quad if \quad q_i > 0 \quad and \quad q_{i-1} > 0 \quad and \quad q_{i+1} = 0 \\ u_{t\ inst(i)} = u_i \quad if \quad q_i > 0 \quad and \quad q_{i-1} = 0 \quad and \quad q_{i+1} > 0 \\ u_{t\ inst(i)} = u_i \quad if \quad q_i > 0 \quad and \quad q_{i-1} = 0 \quad and \quad q_{i+1} = 0 \\ u_{t\ inst(i)} = N/A \ \ all \ \ other \ \ cases \end{array} \tag{3}$$

where $u_{t\ inst\ (i)}$ is the instantaneous threshold at time i, u_i is the wind speed at time i, q_i is the sediment transport at time i, q_{i+1} is the sediment transport at time $i+1$ (in seconds), and q_{i-1} is the sediment transport at time $i-1$ (in seconds). For each 5 min measurement interval, a variety of metrics can be reported to describe the distribution of $u_{t\ inst.}$ values. Row 1 in Eq. (3) approximates the impact threshold and Row 2 in Eq. (3) approximates the fluid threshold as traditionally defined by Bagnold (1941). However, to simplify comparison in this study, we only report the mean of all $u_{t\ inst.}$ values for each measurement interval.

3.4. Regression method

Many investigators have used different regression equations to develop an estimate of threshold. Typically a model is fitted to a dataset with wind speed as explanatory variable and sediment flux as response variable. The explanatory axis intercept where sediment flux is equal to zero is taken as the threshold. A variety of models have been used, for example Arens (1996) and Clifton et al. (2006, snowdrift) used a cubic equation; Gillette et al. (1997b) used an empirical equation, and Schönfeldt (2004) used a linear model with conditionally averaged data.

We investigated a series of models with this dataset. In general, higher exponents (2, 3) produced threshold values that were much lower than other threshold results (e.g., negative, systematically below 3 m s^{-1}). Consequently, we have used linear models throughout.

We performed a linear regression of sediment transport flux and wind speed for each measurement interval. Threshold was taken as the predicted value where sediment transport equals zero (see Fig. 4). We used counts s^{-1} from the piezoelectric sensor as a measure of sediment transport flux and assume linear proportionality between mass flux and count rate (found to be a reasonable assumption for similar sensors by Gillette et al., 1997a and Baas, 2004). It is important to note that the dependability of the regression method rests on the validity of these assumptions. Both count rate and wind speed were treated as continuous measurements in the ordinary least squares regression:

$$q = a\left(u - u_{t\ regression}\right) \tag{4}$$

where q is non-zero sediment transport flux, a is a regression coefficient, u is wind speed, and $u_{t\ regression}$ is the regression threshold, determined as a coefficient in the regression.

4. Mass transport prediction methods

We calculated predicted mass transport to explore the potential implications of using different threshold calculation methods. Mass flux estimates were performed for comparisons made with a fixed measurement interval (5 min). As the purpose of these estimates is simply comparative, we follow common protocols for predicting mass flux. We do not know how these estimates compare to true mass flux; the focus of this study is strictly on comparing the implications of modifying threshold calculation method.

Mass flux was predicted with the Lettau and Lettau (1978) equation. A version of this equation is used in the widely acknowledged 'Fryberger method' (Fryberger, 1979). Any similar equation will produce similar results. For all records where wind speed (u) exceeded threshold wind speed (u_t) the mass flux (q, in kg s^{-1} per crosswind meter) was computed from:

$$q = C\,(d/D)^{0.5}(\rho_a/g)\,(u_* - u_{*t})\,u_*^2 \tag{5}$$

where C is a constant (4.2; from Sherman et al., 1998), d is the grainsize of the study site (≈0.34 mm), D is a reference grainsize (0.25 mm), ρ_a is the air density (held constant at 1.22 kg m^{-3}), g is the acceleration of gravity (9.81 m s^{-2}), u_* and u_{*t} are the surface friction velocity and threshold friction velocity, respectively, which were determined by re-arranging the "Law of the Wall" to:

$$u_* = (\kappa\, u_z) / (\ln(z/z_0)) \tag{6}$$

where κ is von Karman's constant (0.41), u_z is the wind speed at elevation z (1.35 m), and z_0 is the aerodynamic roughness length, which is assumed to be 1/30th of the mean grain size, calculated as 1.13×10^{-5} m (Sherman et al., 1998). The total transport prediction (Q) was calculated with:

$$Q = \sum(300q) \tag{7}$$

where q is the mass flux prediction for each 5 min (300 s) measurement interval. Calculations were repeated for thresholds measured with each method. Note that calculations were only made for measurement intervals with threshold measurements. Following the above methods, transport calculations could only be performed in measurement intervals with intermittent transport.

5. Results

During the 278.31 h deployment, measured sediment transport occurred 20.07 h under a variety of wind speeds. A variety of surface conditions were observed in camera photos, suggesting that threshold changed throughout the deployment. With a measurement interval of 5 min, threshold estimates were possible with all methods in 468 measurement intervals. Within these 468 records the statistics of sediment transport and wind speed are listed in Table 2.

Measured threshold values varied throughout the deployment (Fig. 5). The focus of this study is a comparison of methods to calculate threshold, so the precise causes of threshold variability are not clear and remain unexplored. In general, large scale variability (5 h. scale) in threshold is consistently measured by all threshold methods;

Table 2
Statistics of wind speed and sediment transport for the measurement intervals when threshold was calculated ($n = 468$).

Statistic	Value
Wind speed mean	6.37 m s^{-1}
Wind speed minimum	3.82 m s^{-1}
Wind speed maximum	10.15 m s^{-1}
Mean wind speed standard deviation	1.03 m s^{-1}
Mean saltation seconds (j)	136.0 s
Saltation seconds (j) 25% quartile	46.0 s
Saltation seconds (j) 75% quartile	227.2 s

however, high frequency variability (5 min scale) in threshold differs among methods. The frequency distribution of threshold values for the full deployment is shown in Fig. 6.

To investigate if threshold measurements co-varied, we plotted scatterplots of all combinations of threshold measurements (Fig. 7). As the GTFEM and TFEM are very similar methods, the correlation was strong ($r = 0.977$). The instantaneous method correlated moderately with the TFEM and GTFEM thresholds; however, the regression method did not correlate well with any of the other methods throughout the range of threshold measurement.

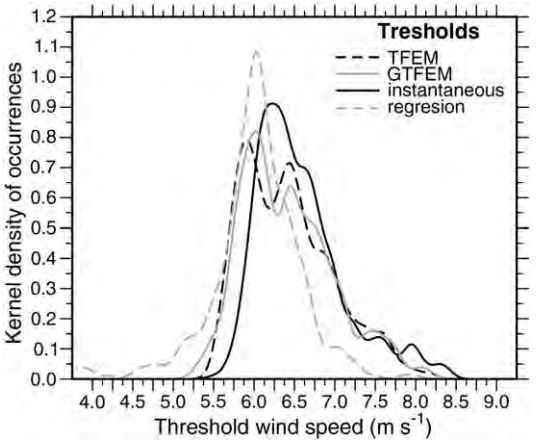

Fig. 6. Kernel density estimates of all thresholds for the full deployment (between 4 and 9 m s^{-1}). Kernel density estimates were performed with the Gaussian kernel, standard deviation = 0.09 m s^{-1}, $n = 468$.

5.1. Mass transport predictions

Large differences in predicted transport occurred (Table 3). The differences matched the systematic trends in threshold calculations. The largest transport predictions occurred with the lowest thresholds (regression method), and the smallest transport predictions occurred with the highest threshold measurements (instantaneous method) (see Fig. 6). Estimates from the TFEM and GTFEM are similar, but not identical.

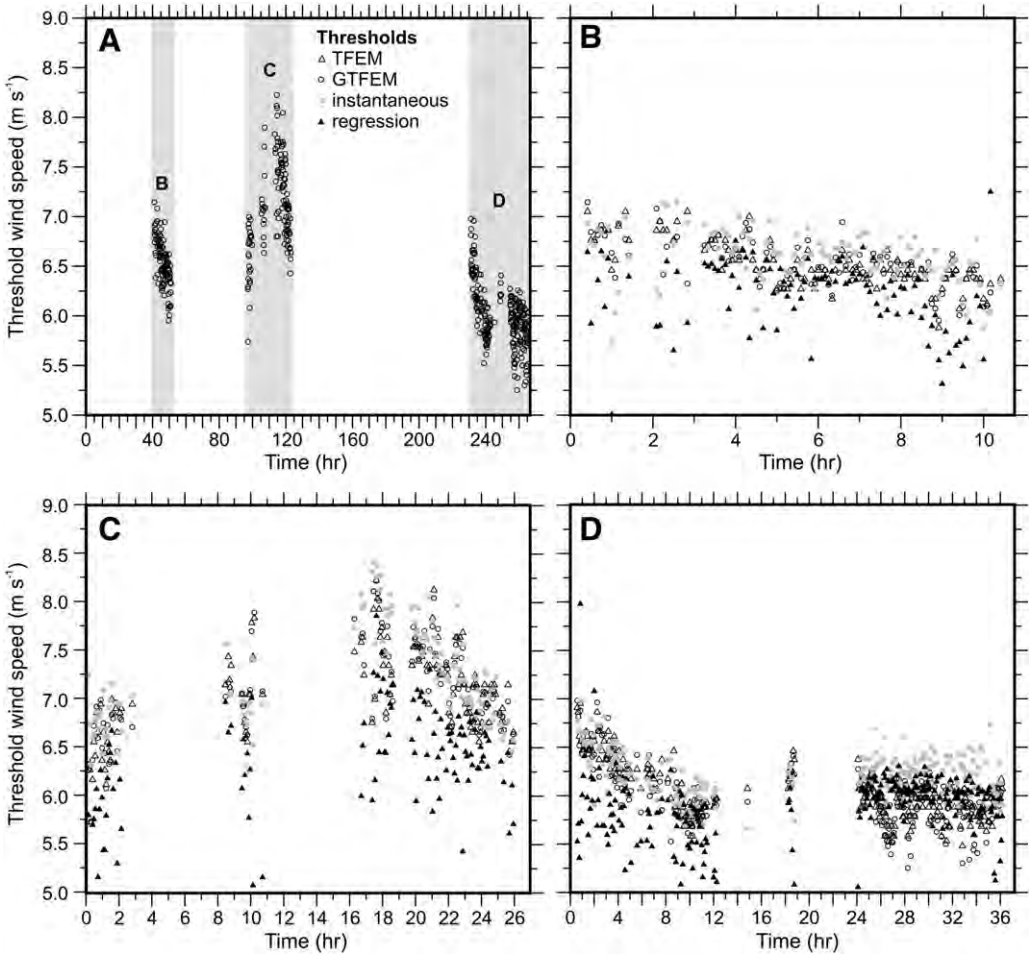

Fig. 5. Threshold wind speeds throughout the deployment. GTFEM threshold is shown for the full deployment (A). Most threshold estimates occurred in one of three distinct time periods. Each time period is shown in more temporal detail in (B), (C), and (D). Threshold wind speeds are measured at 1.35 m height.

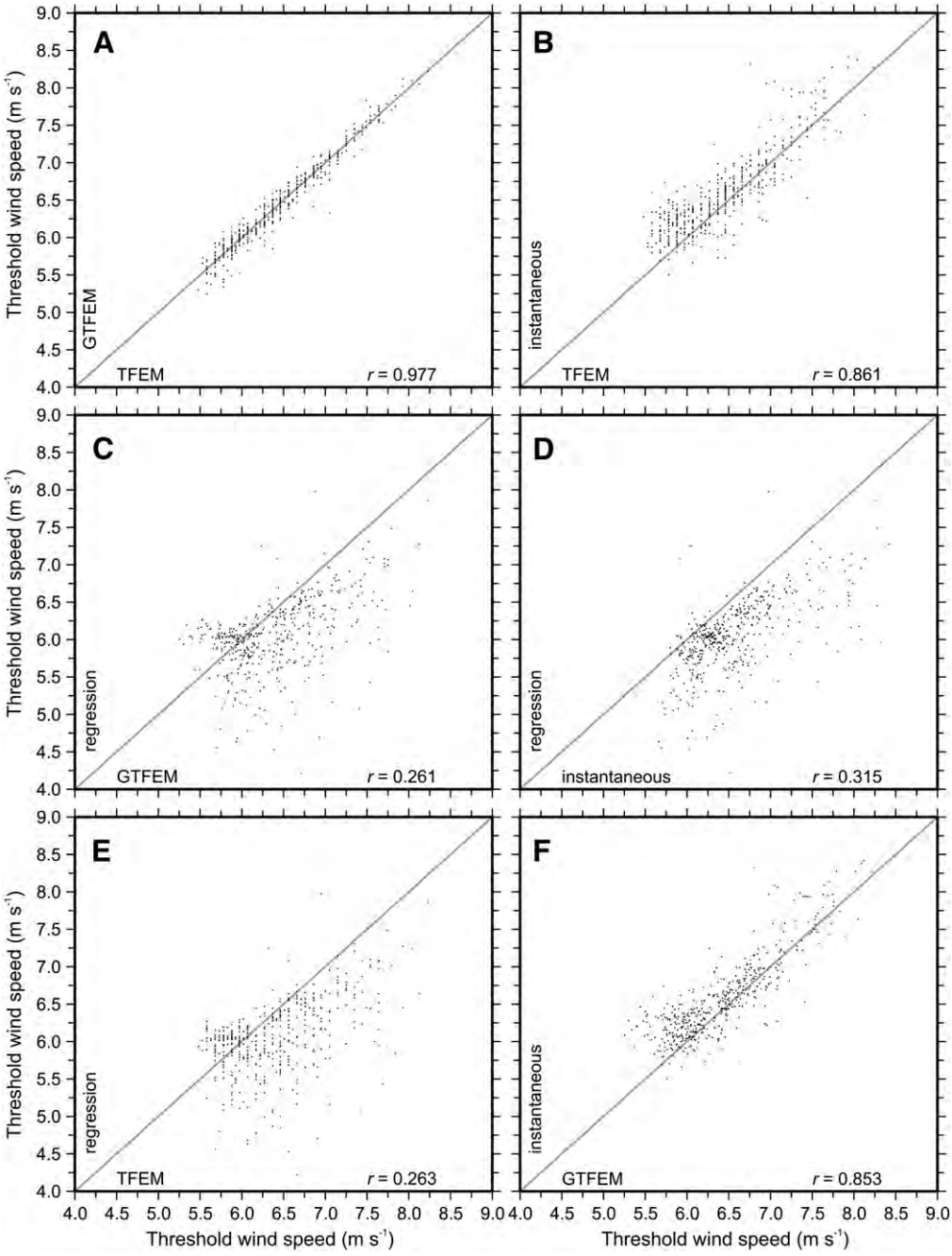

Fig. 7. Method to method comparisons of calculated threshold wind speeds. Gray lines are 1:1. Only shown are thresholds between 4 and 9 m s^{-1}, r = Pearson's correlation coefficient (calculated with all data; $n = 468$). Note these results are deployment specific and cannot be used to correct threshold measurements.

5.2. Modifications of measurement interval

We calculated thresholds for the dataset with a variety of measurement intervals (Fig. 8). Increasing the measurement interval resulted in a systematic decrease in thresholds calculated with the GTFEM, TFEM, and instantaneous methods. The regression method thresholds did not change appreciably beyond a measurement interval of 300 s. The 25% to 75% quartile range of all threshold calculation methods decreased with an increase in measurement interval suggesting there is less variability in measured thresholds with an increase in measurement interval. There was preferential binning in TFEM threshold results (straight horizontal lines in Fig. 8A) due to the resolution limitations of the TFEM (0.049 m s^{-1} in this study).

Table 3
Predicted mass transport for measurement intervals when threshold was calculated ($n = 468$).

Threshold calculation method	Predicted mass transport (kg per crosswind meter)
TFEM	95.92
GTFEM	93.60
Instantaneous method	63.57
Regression method	126.62

6. Discussion

Variability in measured threshold values suggests that the actual threshold was variable over the 11 day deployment (Figs. 5–7). The

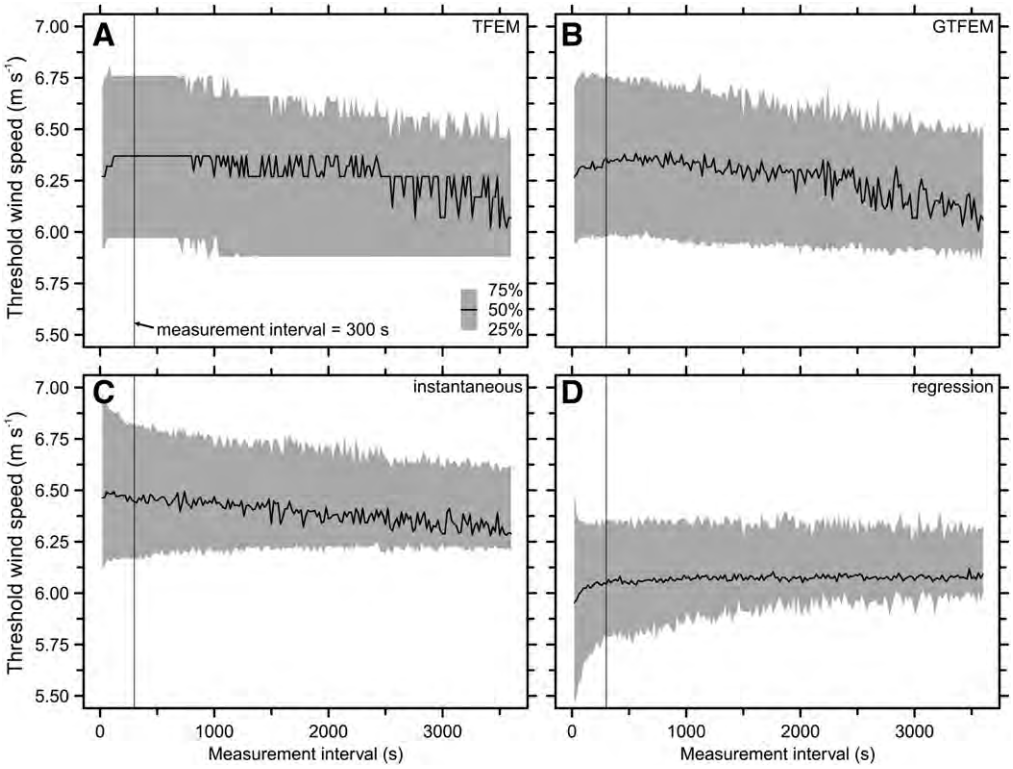

Fig. 8. The distribution of threshold measurements as measurement interval is modified for each threshold calculation method. Black line is median, gray area is 25% to 75% quartiles. Note these results are deployment specific.

source of threshold variability is unclear. It is likely that threshold variability is controlled by complex spatio-temporal interactions among surface moisture (e.g., Fig. 2), air temperature, relative humidity, and turbulence characteristics (similar to findings from studies listed in Table 1). Although unexplained, the variability in measured thresholds supports the underlying motivation of this study. If threshold variability is pervasive (e.g., Fig. 5), future investigators will require reliable methods to accurately and consistently measure this variability.

The threshold methods did not produce identical measurements (Fig. 5). Intuitively, this can be expected as each method is based on a different set of assumptions and generalizations of the threshold concept. Although the differences may appear minor (ranging 0.5–2.0 m s^{-1}; Figs. 5 and 6), threshold is an important non-linearity in most sediment flux formulae (e.g. Eq. (5)). The discrepancy resulted in non-negligible differences in estimated mass transport (Table 3). It is important to note that these results are deployment- and sensor-specific; these values can only be used to illustrate the *presence* of differences among methods. These results do not represent a reliable estimate of the magnitude of differences and cannot be used as a correction factor. Regardless of these limitations, the very existence of non-negligible differences in this relatively routine deployment suggests that results from different threshold calculation methods are incommensurate.

These results are similar to those published by Stout (1998), Wiggs et al. (2004a) and Barchyn and Hugenholtz (2010). All studies showed that modifying aspects of the measurement system modified measured threshold values. Calibrating results from one measurement system to another is likely to be difficult given the poorly understood nature of natural sediment transport (Baas and Sherman, 2005). Even the most simple of modifications (e.g., anemometer type) can similarly affect threshold values (Barchyn and Hugenholtz, unpublished data).

The source of differences among threshold calculation methods is very difficult to conclusively determine. Underlying each of the threshold calculation methods is a series of assumptions and generalizations. It is difficult to determine which generalizations are more accurate than others. This poses a challenge for determining the 'best' threshold method. However, it is possible to discuss the *reliability* of assumptions underlying individual threshold calculation methods. We first discuss the comparability and reliability of each threshold calculation method prior to exploring potential strategies that may improve field-based threshold measurement.

6.1. Comparability and reliability of TFEM and GTFEM thresholds

Both the TFEM and GTFEM require the investigator to generalize the threshold concept over the measurement interval. This generalization implies that all instances of sediment transport occur at wind speeds above threshold and all instances with no transport occur at wind speeds below threshold. The dynamics of the sample calculation dataset (Figs. 3 and 4) provide evidence that the beginning and ending of sediment transport bursts can occur at wind speeds above and below threshold. Wiggs et al. (2004a) found similar results, in that sediment transport could occur at wind speeds below the TFEM threshold and instances of no sediment transport occurred when wind speeds were above the TFEM threshold. As a solution, Wiggs et al. (2004a) recommended using a 40 s sampling (or 'averaging') interval instead of 1 Hz, which was found to be optimum for their deployment. Regardless of the precise choice in sampling interval, it is clear that the presence and absence of sediment transport rarely follows the notion of a threshold precisely. There is substantial high-frequency variability in the wind speed corresponding with the beginning or ending of transport (Figs. 3 and 4).

The GTFEM differs from the TFEM by the assumption of a synthetic wind speed distribution. The close correlation between the two methods (Fig. 7A) suggests that the wind speed distributions during the field deployment were commonly close to Gaussian. To assess this in more detail, we calculated skew and kurtosis for each measurement

interval to examine the systematic trends in the shape of wind speed distributions throughout the deployment (Fig. 9).

The distributions of wind speeds in measurement intervals were systematically positively skewed and platykurtic in comparison to a Gaussian distribution. Because these results are deployment-specific, we hesitate to draw extensive conclusions regarding the applicability of assuming a Gaussian wind speed distribution. However, the comparability of TFEM and GTFEM results explicitly relies upon the assumption that wind speed distributions are Gaussian. This assumption may be valid in certain deployments; however, in other deployments error could be much larger than seen here. As noted by Stout (2004), skew and kurtosis could be calculated and used to assess the quality of threshold estimates; however, this practice would likely restrict the number of threshold estimates. It may be more straightforward and reliable to use the TFEM method exclusively. If desired, the TFEM can be calculated directly in most dataloggers with a slightly more complicated program that records wind speeds into an array and references elements in the array (per Eq. (1)) at the end of the measurement interval.

6.2. Reliability of the instantaneous method threshold

The instantaneous method is a different interpretation of the threshold concept. Instead of generalizing the threshold concept over a measurement interval, the instantaneous method extracts the individual wind speeds associated with the 'event' of a threshold being passed (e.g., transport beginning or ending). It is not clear if the 'event' of a threshold being passed is the 'threshold' that was designed for use in transport models. Some argue that these events could be mostly driven by streamers or other factors than local surface erodibility (Baas and Sherman, 2005; R. Davidson-Arnott, pers. comm., 2010). Furthermore, wind speed measured at some height above the surface (at a high resolution) may not be fully representative of shear stress at the surface. Variability in wind profile is common with turbulence.

The number of instantaneous method thresholds that are averaged for a given measurement interval could vary from one to many, depending on the level of transport intermittency. Consequently, non-systematic variability in results attributed to measurement system precision (e.g., anemometer precision, differences between wind at height and surface, sediment transport sensor precision) may not be averaged enough. These limitations could be addressed with different generalization techniques (e.g., *k*-nearest neighbors, moving window averaging), or by enforcing a minimum number of instantaneous threshold measurements per measurement interval.

The instantaneous method, although not fully tested, could straightforwardly be modified to develop frequency distributions of 'threshold events' in space and time over a dune surface (as suggested by Davidson-Arnott et al., 2008; Zhen-shan et al., 2008). Both the fluid and impact thresholds can be extracted separately. The method shows promise and certainly could yield interesting information from a phenomenological perspective; however, more work is required to understand the intricacies of measuring 'threshold events' at high resolution.

6.3. Reliability of the regression method threshold

The regression method is a generalization approach that requires the investigator to assume that the relation between wind and sediment transport follows a particular model. In this study we used a linear model. Most transport models in aeolian geomorphology conceptualize transport rate to be proportional to the cube of wind speed (e.g., see review by Sherman et al., 1998). Models with larger coefficients (2–3) tended to produce threshold intercepts that were anomalously low, the cause of which remains to be determined. It could be an artifact of the technique or sensors, or the relation between wind speed and sediment transport could be closer to linear than most transport models assume (R. Davidson-Arnott, pers. comm., 2010).

To demonstrate this method we were forced to assume that the relation between sediment transport and sensor count rate is approximately linear. Although previous investigators have cautiously made this assumption (tested by Gillette et al., 1997a; Baas, 2004), we are hesitant given recent studies that have found inconsistent response with piezoelectric sensors (Baas, 2004; Van Pelt et al., 2009; Barchyn and Hugenholtz, 2010). Further work is required to ensure that high resolution sediment transport sensors are calibrated, consistent, and tested robustly (Baas, 2008).

The second major assumption is that the relation between wind and sediment transport follows a particular model. Recent work exploring the relation between various aspects of turbulence and transport (e.g., Baas and Sherman, 2005; Ellis, 2006; Weaver and Wiggs, 2011) has shown that coherent turbulence structures and streamer dynamics may be an important explanatory variable in transport modeling. Consequently, the simplification of any straightforward time-independent relation between wind speed and sediment transport could be too simple to be reliable at the 1 Hz scale.

6.4. Modifications of measurement interval

We calculated thresholds for a number of different measurement intervals (Fig. 8). We are hesitant to draw broad conclusions from these data because these results are highly deployment specific; however, there are some general trends that may be reproducible. The variability decreased with all methods as measurement interval increased. This is expected as there is high frequency variability in threshold (Fig. 5; also noted by Stout, 2004; 2007). Increasing the measurement interval suppresses this high frequency variability.

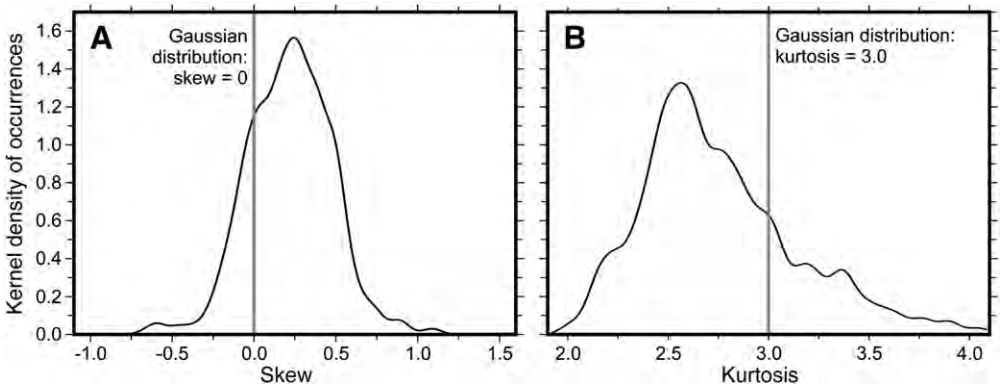

Fig. 9. A) Kernel density estimate of skew values for each 5 min measurement interval ($n = 468$, Kernel: Gaussian, standard deviation = 0.05 m s^{-1}). B) Kernel density estimate of kurtosis values for each 5 min measurement interval ($n = 468$; Kernel: Gaussian, standard deviation = 0.05 m s^{-1}).

Modifying the measurement interval results in a different interpretation of threshold (at a different scale) and should be held constant if investigators wish to compare results.

The source of high-frequency variability in threshold measurements is not clear. Stout (2004) hypothesized that this variability was due to dry and wet patches on the sediment surface. The dynamics of moisture on a dune surface (as an explanatory variable of threshold) are very fast (minutes; Davidson-Arnott and Bauer, 2009); consequently, investigators should match the scale of threshold measurement to the scale of the explanatory variables. We are hesitant with larger measurement intervals, unless it can be shown that the dominant controls of threshold are larger scale (e.g., large scale aerodynamic roughness changes, Wiggs and Holmes, in press).

6.5. Potential strategies to address threshold incomparability

Following previous works (Stout, 1998; Wiggs et al., 2004a; Barchyn and Hugenholtz, 2010) we have demonstrated that modifying aspects of the field-based threshold measurement system can result in non-negligible differences in results. Together, these findings suggest that there are a number of individual definitions of 'threshold' in use, none of which are directly comparable. This could pose a challenge for applying these threshold measurements in transport formulae. Nevertheless, there are several strategies that may improve this situation.

6.5.1. Semantic clarification

First, we believe that the semantics of threshold determination should be clarified. Instead of referring to all these measurements with one name ('threshold'), we suggest referring to these measurements as individual erodibility metrics, complete with metadata on the measurement system. For example, in this study we have reported values that should be referred to as 'TFEM erodibility, measurement interval: 5 min; sampling interval: 1 Hz; transport measurements: Sensit H11-B, 0.05 m height; wind measurements: RM Young 5103, 1.35 m height'. This clarification of semantics could help prevent these measurements from being applied in unintended applications following the publication of a given study. We find the present situation confusing for investigators as there are a number of interpretations of the same concept (all named 'threshold') and it is not clear whether these results can be compared, synthesized, or applied.

6.5.2. Threshold measurement standardization

Although clarifying the semantics of threshold measurement may help distinguish different interpretations of the 'threshold' concept, it does not improve the applicability or comparability of these threshold values. We doubt that reliable calibration methods can be developed to modify threshold values measured with different calculation methods (or sensors; Barchyn and Hugenholtz, 2010) due to the complexity of natural sediment transport (Baas and Sherman, 2005; Davidson-Arnott and Bauer, 2009). We believe each of the studies in Table 1, are in essence 'case studies', where although measurements are made, the measurements have limited quantitative applicability outside of the study. A promising approach that investigators may wish to consider is the development of technical standards (Lal, 1994).

Standards could help investigators provide empirical answers to comparative questions that are presently challenging to answer; for example: how does threshold vary between coastal (e.g., Davidson-Arnott and Bauer, 2009) and inland sites (e.g., this study)? This question is difficult to answer with the present diversity of threshold measurement systems in use. Studies in Table 1 present variability in threshold data that are in most cases not fully explained. As discussed by many investigators (e.g., Wiggs et al., 2004b; Davidson-Arnott and Bauer, 2009), natural threshold variability is poorly understood. We believe more empirical data could help. Standards could add value and longevity to threshold measurements, allowing the results from many studies to be synthesized; this could aid future researchers develop more reliable prediction models that will function across environments. However, the concept requires some discussion among investigators.

The applicability of field-based threshold measurements in transport formulae requires some consideration. Transport formulae originally designed to function with an analytical threshold model (e.g., Bagnold, 1941) as an input for u_{*t} may require some re-tuning (perhaps a modification to the empirical constants). Such a process is vastly simplified with one standard method.

The development of a standard method is a challenging task. At a minimum, all of the aspects of the measurement systems listed as columns in Table 1 would require specification. We believe that standards require discussion within the community; however, we will tentatively make some recommendations for consideration.

Of the methods tested here, the TFEM of Stout and Zobeck (1996, 1997) has seen the widest use and likely has the most reliable assumptions. The 1 Hz sampling interval is practical and widely used (c.f., Wiggs et al., 2004a). A measurement interval of 5 min is also practical. The dynamics of surface moisture in moist aeolian environments operate at this temporal scale, and a threshold measurement method should measure variability at a scale similar to the dynamics of explanatory variables (discussed further in Section 6.4).

It is widely acknowledged that the lack of consistent and quality sensors for aeolian sediment transport is a great challenge (Baas, 2004; 2008; Van Pelt et al., 2009; Barchyn and Hugenholtz, 2010). We believe piezoelectric sensors have yet to be demonstrated as consistent enough for choice as a standard; a more consistent alternative for consideration is the Wenglor YH03PCT08 (see Hugenholtz and Barchyn, 2011). In essence, a standard sensor provides a standard definition of the 'presence of sediment transport' in the conceptualization of threshold as 'the minimum wind speed for the presence of sediment transport'. Inconsistency in the definition of the 'presence of sediment transport' (indirectly introduced by many different sensors) has been acknowledged to be a pervasive issue affecting comparability of most aspects of threshold measurement (Lyles and Krauss, 1971; Fécan et al., 1999, Zhen-shan et al., 2008; Barchyn and Hugenholtz, 2010). Most investigators measuring threshold have implicitly defined the 'presence of sediment transport' with the sensors used and in most cases metadata on the definition (e.g., characteristics of the sensor) remain undocumented. The height of transport sensor mounting may be dominated by practicalities: transport sensors mounted lower than 0.05 m can be quickly buried (Barchyn and Hugenholtz, unpublished data), leading to long periods of no data until the sensor can be remounted. Future research is essential to understand the potential impact of sensor positioning on threshold values during unattended deployments (see Ellis et al., 2009 for discussion of the notable impact of sensor height on mass flux profiles). Regardless, the height and status of sediment transport sensors should be monitored with time-lapse cameras continuously to quality control the data.

Choice of anemometer is likely less important as anemometer technology is much more developed than sediment transport sensor technology. The RM Young 5103 propeller is widely available, relatively inexpensive, and fast responding. Practically, an anemometer height of 1–2 m is above most transport, this preserves anemometer life (indirectly reducing research costs and improving spatial resolution).

Technical standards could be a practical approach to improve inter-study comparability and inter-environment empirical modeling; however, at this point we are simply advocating for a discussion of the idea. We believe researchers of the applied aspects of aeolian sediment transport (e.g., agricultural wind erosion) could immediately benefit from a standard method; whereas other investigators could simultaneously research new conceptualizations of threshold. The two approaches need not be mutually exclusive.

6.6. Re-conceptualizations of field-based thresholds

Threshold is commonly conceptualized as a property of the local surface (e.g., grain size, moisture, crusting, etc.). Most studies of threshold attempt to relate some local surface condition to threshold variability. In field deployments, however, there is evidence suggesting that this conceptualization is not as reliable as in wind tunnels. Here we discuss several criticisms of the field-based threshold methods and propose a re-conceptualization of threshold in order to clarify its representation of transport conditions under natural winds.

A widely acknowledged time-dependent aspect of threshold phenomenon is the fluid and impact thresholds of Bagnold (1941). All threshold calculation methods compared in this study produce an averaged 'single value threshold', which can be criticized (Schönfeldt, 2004). The fluid and impact thresholds can be isolated with the instantaneous method (see Section 3.3); however, it is important to consider the practicality of these measurements. At present, most transport modeling frameworks are time-independent (e.g., Eq. (5)). Modeling transport with time-dependent threshold will require investigators to model transport numerically, simulating the response of the system to each gust and lull in wind speed (e.g., Schönfeldt, 2004). This may not be practical for larger scale applications, and we believe more high resolution empirical transport data would be required to validate this type of prediction framework than is presently available (data similar to Baas and Sherman, 2005).

A second criticism of field-based threshold measurement methods is that a single value doesn't provide an adequate representation of the threshold concept; a better representation is a distribution of values. Although this idea has seen healthy discussion (Nickling, 1988; Davidson-Arnott et al., 2005; 2008; Zhen-shan et al., 2008), it is not clear precisely how such a parameterization would be developed empirically or applied in transport models (see Zhen-shan et al., 2008 for an discussion of an analytical approach). These distributions could be straightforwardly measured and generalized in time (e.g., within a moving window); however, careful consideration is required when picking the size of the moving window as it controls the scale of threshold generalization.

A third criticism is based on the implicit assumption that a measured threshold represents the erodibility of the local surface. There are many situations in natural transport environments where the presence of transport (or 'threshold') is caused by explanatory variables other than local shear stress exceeding the local erodibility. Fig. 10 shows an illustration demonstrating hypothetical (but common, e.g. see Fig. 2) situations where a 'threshold' is measured, but the measurement may not be a function of local erodibility.

A potential solution is a re-conceptualization of measured field-thresholds as a function of more than strictly the local surface conditions. Several additional explanatory variables could include: (i) variability in upwind supply and erodibility (e.g., Fig. 10), (ii) some coherent aspect of turbulence (e.g., Ellis, 2006; Weaver and Wiggs, 2011), and/or (iii) characteristics of streamer dynamics (Baas and Sherman, 2005). The local surface conditions may play a relatively minor role in measured threshold variability. In this conceptualization, investigators could describe thresholds as a distribution, but we caution that this distribution may not be strictly attributable to variability in the surface entrainment susceptibility (as proponents of the distribution approach argue: e.g., Zhen-shan et al., 2008; Davidson-Arnott et al., 2005; 2008). The distribution could simply represent empirical indeterminacy which may not be attributable to any specific explanatory variable (see discussion of indeterminacy by Bauer et al., 1996). Finally, if this re-conceptualization is adopted, investigators should avoid comparison with analytical or wind-tunnel derived thresholds; field-based threshold measurements would be a fundamentally different measurement. Overall, we believe investigators should carefully consider the source of variability in field-measured thresholds; the entrainment of sediment in natural environments may be due to much more than the local surface conditions adjacent to the sensor.

7. Conclusions

We compared four methods of calculating aeolian sediment transport threshold from identical raw field data. Results suggest that the methods produce values that are similar but not commensurate. This inconsistency can affect predictions of mass transport.

We discussed several strategies that could help investigators evolve methods for measurement of field-based thresholds. We discussed comparability of field-based thresholds and are hesitant to recommend comparing any field-based threshold value with any other value. This could challenge the development of models that are reliably developed and tested with data from multiple environments.

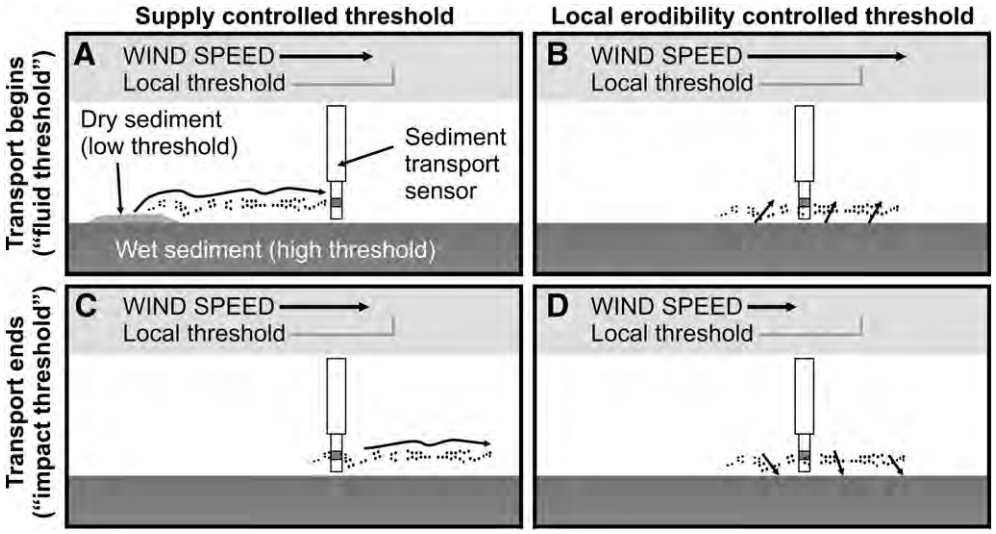

Fig. 10. In natural environments transport can begin or end (passing of a 'threshold') in a variety of situations that may not be related to the local erodibility. Local wind speed (length proportional to speed) and entrainment threshold (directly adjacent to the sensor) is denoted with arrow and gray marking at the top if each panel. The beginning of a transport burst can occur in two situations: (A) a dry patch of sediment upwind is eroded at a lower windspeed than the local threshold, or (B) the wind entrains sediment locally. The end of a transport burst can occur in two situations: (C) supply eroded from some upwind source is depleted, wind speed is insufficient to entrain sediment locally, or (D) wind speed drops below impact threshold necessary to maintain transport. Field measurements of threshold could be re-conceptualized to be a function of more than simply the local erodibility.

We recommend clarifying the semantics associated with threshold measurement. Another potential solution is the development of a standard method; however, a standard method would require specification of almost every aspect of the measurement system. Several re-conceptualizations of 'threshold' could provide complementary insight into the controls of threshold dynamics. For example, threshold could be described within a time-dependent framework, as a distribution of values, or be conceptualized as a function of more than the local surface conditions.

Threshold, in general, remains a parameter that is difficult to measure in the field. Despite this, it is necessary to venture into the field to gain a true picture of threshold and its controls and dynamics. Empirical data is a necessary component of this research. A renewed and careful focus on the methods for threshold measurement will help future investigators develop more robust transport models that will benefit all aspects of aeolian geomorphology.

Acknowledgements

This research was funded by the University of Lethbridge, Natural Sciences and Engineering Research Council of Canada, and Alberta Innovates. This manuscript was improved by discussions with Matthew Letts, René W. Barendregt, Stefan Kienzle, and Dan Johnson. Helpful suggestions by editor Andrew Plater, Robin Davidson-Arnott and one anonymous reviewer are greatly appreciated. Dune GIS data in Fig. 1B are courtesy Stephen A. Wolfe. GIS data for Fig. 1C are courtesy the Government of Saskatchewan, Canada.

References

Ahlbrandt, T.S., 1979. Textural parameters of Aeolian deposits. In: McKee, E.D. (Ed.), A Study of Global Sand Seas: United States Geological Survey Professional Paper, 1052, pp. 305–397.
Arens, S., 1996. Rates of aeolian transport on a beach in a temperate humid climate. Geomorphology 17, 3–18.
Argaman, E., Singer, A., Tsoar, H., 2006. Erodibility of some crust forming soils/sediments from the Southern Aral Sea Basin as determined in a wind tunnel. Earth Surf. Processes Landforms 31, 47–63.
Baas, A.C.W., 2004. Evaluation of saltation flux impact responders (Safires) for measuring instantaneous aeolian sand transport intensity. Geomorphology 59, 99–118.
Baas, A.C.W., 2008. Challenges in aeolian geomorphology: investigating aeolian streamers. Geomorphology 93, 3–16.
Baas, A.C.W., Sherman, D.J., 2005. Formation and behaviour of Aeolian streamers. J. Geophys. Res. 110, F03011.
Bagnold, R.A., 1941. The Physics of Blown Sand and Desert Dunes. Methuen, London.
Barchyn, T.E., Hugenholtz, C.H., 2010. Field comparison of four piezoelectric sensors for detecting aeolian sediment transport. Geomorphology 120, 368–371.
Bauer, B.O., Davidson-Arnott, R.G.D., Nordstrom, K.F., Ollerhead, J., Jackson, N.L., 1996. Indeterminacy in aeolian transport across beaches. J. Coastal Res. 12, 641–653.
Clifton, A., Ruedi, J.D., Lehning, M., 2006. Snow saltation threshold measurements in a drifting-snow wind tunnel. J. Glaciol. 52, 585–596.
Darke, I., McKenna Neuman, C., 2008. Field study of beach water content as a guide to wind erosion potential. J. Coastal Res. 24, 1200–1208.
Davidson-Arnott, R.G.D., Bauer, B.O., 2009. Aeolian sediment transport on a beach: thresholds, intermittency, and high frequency variability. Geomorphology 105, 117–126.
Davidson-Arnott, R.G.D., MacQuarrie, K., Aagaard, T., 2005. The effect of wind gusts, moisture content and fetch length on sand transport on a beach. Geomorphology 68, 115–129.
Davidson-Arnott, R.G.D., Yang, Y., Ollerhead, J., Hesp, P.A., Walker, I.J., 2008. The effects of surface moisture on aeolian sediment transport threshold and mass flux on a beach. Earth Surf. Processes Landforms 33, 55–74.
De Oro, L.A., Buschiazzo, D.E., 2009. Threshold wind velocity as an index of soil susceptibility to wind erosion under variable climatic conditions. Land Degrad. Dev. 20, 14–21.
Delgado-Fernandez, I., Davidson-Arnott, R.G.D., Ollerhead, J., 2009. Application of a remote sensing technique to the study of coastal dunes. J. Coastal Res. 25, 1160–1167.
Dyke, A.S., Prest, V.K., 1987. Late Wisconsinan and Holocene history of the Laurentide ice sheet. Géogr. Phys. Quatern. 41, 237–263.
Ellis, J.T., 2006. Coherent structures and aeolian saltation. PhD thesis, Texas A & M University, College Station, TX, USA.
Ellis, J.T., Li, B., Farrell, E.J., Sherman, D.J., 2009. Protocols for characterizing aeolian mass-flux profiles. Aeolian Res. 1, 19–26.
Farrell, E.J., Sherman, D.J., 2006. Process-scaling issues for aeolian transport modelling in field and wind tunnel experiments: roughness length and mass flux distributions. J. Coastal Res. SI 39, 384–389.
Fécan, F., Marticorena, B., Bergametti, G., 1999. Parameterization of the increase of the aeolian erosion threshold wind friction velocity due to soil moisture for arid and semi-arid areas. Ann. Geophys. 17, 149–157.
Fryberger, S.G., 1979. Dune forms and wind regime. In: McKee, E.D. (Ed.), A Study of Global Sand Seas: United States Geological Survey Professional Paper, 1052, pp. 137–169.
Fryrear, D., Bilbro, J., Saleh, A., Schomberg, H., Stout, J.E., Zobeck, T.M., 2000. RWEQ: improved wind erosion technology. J. Soil Water Conserv. 55, 183–189.
Gillette, D.A., Fryrear, D.W., Xiao, J.B., Stockton, P., Ono, D., Helm, P.J., Gill, T.E., Ley, T., 1997a. Large-scale variability of wind erosion mass flux rates at Owens Lake. 1. Vertical profiles of horizontal mass fluxes of wind-eroded particles with diameter greater than 50 μm. J. Geophys. Res. 102, 25977–25987.
Gillette, D.A., Hardebeck, E., Parker, J., 1997b. Large-scale variability of wind erosion mass flux rates at Owens Lake, 2. Role of roughness change, particle limitation, change of threshold friction velocity, and the Owen effect. J. Geophys. Res. 102, 25989–25998.
Howard, A.D., 1977. Effect of slope on the threshold of motion and its application to orientation of wind ripples. Geol. Soc. Am. Bull. 88, 853–856.
Hugenholtz, C.H., Barchyn, T.E., 2011. Laboratory and field performance of a laser particle counter for measuring aeolian sand transport. J. Geophys. Res.-Earth. 116, F01010.
Hugenholtz, C.H., Wolfe, S.A., 2005. Recent stabilization of active sand dunes on the Canadian prairies and relation to recent climate variations. Geomorphology 68, 131–147.
Hugenholtz, C.H., Wolfe, S.A., Walker, I.J., Moorman, B.J., 2009. Spatial and temporal patterns of aeolian sediment transport on an inland parabolic dune, Bigstick Sand Hills, Saskatchewan, Canada. Geomorphology 105, 158–170.
Klassen, R., 1994. Late Wisconsinan and Holocene history of southwestern Saskatchewan. Can. J. Earth Sci. 31, 1822–1837.
Lal, R., 1994. Soil Erosion Research Methods. Soil Water Conservation Society. St. Lucie Press, Delray Beach, Florida, USA.
Lancaster, N., Helm, P., 2000. A test of a climatic index of dune mobility using measurements from the Southwestern United States. Earth Surf. Processes Landforms 25, 197–207.
Larney, F.J., Bullock, M.S., McGinn, S.M., Fryrear, D.W., 1995. Quantifying wind erosion on summer fallow in southern Alberta. J. Soil Water Conserv. 50, 91–95.
Lettau, K., Lettau, H.H., 1978. Experimental and micrometeorological studies of dune migration. In: Lettau, K., Lettau, H.H. (Eds.), Exploring the world's driest climate. University of Wisconsin INSTITUTE of Environmental Science, Madison, WI, USA, pp. 110–147.
Li, J., Okin, G.S., Herrick, J.E., Belnap, J., Munson, S.M., Miller, M.E., 2010. A simple method to estimate threshold friction velocity of wind erosion in the field. Geophys. Res. Lett. 37, L10402.
Lyles, L., Krauss, R.K., 1971. Threshold velocities and initial particle motion as influenced by air turbulence. T. Am. Soc. Agr. Eng. 14, 563–566.
Marticorena, B., Bergametti, G., 1995. Modeling the atmospheric dust cycle: 1. Design of a soil-derived dust emission scheme. J. Geophys. Res. 100, 16415–16430.
McKenna Neuman, C., 1990. Role of sublimation in particle supply for aeolian transport in cold environments. Geogr. Ann. 72, 329–335.
McKenna Neuman, C., Lancaster, N., Nickling, W.G., 2000. The effect of unsteady winds on sediment transport on the stoss slope of a transverse dune, Silver Peak, NV, USA. Sedimentology 47, 211–226.
Nickling, W.G., 1988. The initiation of particle movement by wind. Sedimentology 35, 499–511.
Nickling, W.G., McKenna Neuman, C., 1997. Wind tunnel evaluation of a wedge-shaped aeolian sediment trap. Geomorphology 18, 333–345.
Nield, J.M., Wiggs, G.F.S., Squirrell, R.S., 2011. Aeolian sand strip mobility and protodune development on a drying beach: examining surface moisture and surface roughness patterns measured by terrestrial laser scanning. Earth Surf. Proc. Land. 36, 513–522.
R Development Core Team, 2009. R: A language and environment for statistical computing, Version 2.10.1. R Foundation for Statistical Computing, Vienna, Austria.
Ravi, S., D'Odorico, P.D., 2005. A field-scale analysis of the dependence of wind erosion threshold velocity on air humidity. Geophys. Res. Lett. 32, L21404.
Sankey, J.B., Germino, M.J., Glenn, N.F., 2009a. Aeolian sediment transport following wildfire in sagebrush steppe. J. Arid Environ. 73, 912–919.
Sankey, J.B., Germino, M.J., Glenn, N.F., 2009b. Relationships of post-fire aeolian transport to soil and atmospheric conditions. Aeolian Res. 1, 75–85.
Schönfeldt, H.J., 2004. Establishing the threshold for intermittent aeolian sediment transport. Meteorol. Z. 13, 437–444.
Sherman, D.J., Farrell, E.J., 2008. Aerodynamic roughness lengths over movable beds: comparison of wind tunnel and field data. J. Geophys. Res. 113, F02S08.
Sherman, D.J., Jackson, D.W.T., Namikas, S.L., Wang, J., 1998. Wind-blown sand on beaches: an evaluation of models. Geomorphology 22, 113–133.
Spaan, W.P., van den Abeele, G.D., 1991. Wind borne particle measurements with acoustic sensors. Soil Technol. 4, 51–63.
Speirs, J.C., McGowan, H.A., Neil, D.T., 2008. Meteorological controls on sand transport and dune morphology in a polar-desert: Victoria Valley, Antarctica. Earth Surf. Processes Landforms 33, 1875–1891.
Stockton, P.H., Gillette, D.A., 1990. Field measurement of the sheltering effect of vegetation on erodible land surfaces. Land Degrad. Rehabil. 2, 77–85.
Stout, J.E., 1998. Effect of averaging time on the apparent threshold for aeolian transport. J. Arid Environ. 39, 395–401.
Stout, J.E., 2004. A method for establishing the critical threshold for aeolian transport in the field. Earth Surf. Processes Landforms 29, 1195–1207.

Stout, J.E., 2007. Simultaneous observations of the critical aeolian threshold of two surfaces. Geomorphology 85, 3–16.
Stout, J.E., 2010. Diurnal patterns of blowing sand. Earth Surf. Processes Landforms 35, 314–318.
Stout, J.E., Zobeck, T.M., 1996. Establishing the threshold condition for soil movement in wind eroding fields. Proc. of the Int. Conf. on Air Pollution from Agricultural Operations 65–85.
Stout, J.E., Zobeck, T.M., 1997. Intermittent saltation. Sedimentology 44, 959–970.
Udo, K., 2009. New method for estimation of aeolian sand transport rate using ceramic sand flux sensor (UD-101). Sensors 9, 9058–9072.
Udo, K., Kuriyama, Y., Jackson, D.W.T., 2008. Observations of wind-blown sand under various meteorological conditions at a beach. J. Geophys. Res. 113, F04008.
Van Pelt, R.S., Peters, P., Visser, S., 2009. Laboratory wind tunnel testing of three commonly used saltation impact sensors. Aeolian Res. 1, 55–62.
Weaver, C.M., Wiggs, G.F.S., 2011. Field measurements of mean and turbulent airflow over a barchan sand dune. Geomorphology 128, 32–41.
Wiggs, G.F.S., Holmes, P., in press. Dynamic controls on wind erosion and dust generation on west-central Free State agricultural land, South Africa. Earth Surf. Proc. Land.
Wiggs, G.F.S., Atherton, R.J., Baird, A.J., 2004a. Thresholds of aeolian sediment transport: establishing suitable values. Sedimentology 51, 95–108.
Wiggs, G.F.S., Baird, A.J., Atherton, R.J., 2004b. The dynamic effects of moisture on the entrainment and transport of sand by wind. Geomorphology 59, 13–30.
Wolfe, S.A., Nickling, W.G., 1993. The protective role of sparse vegetation in wind erosion. Prog. Phys. Geog. 17, 50–68.
Wolfe, S.A., Huntley, D.J., David, P.P., Ollerhead, J., Sauchyn, D.J., MacDonald, G.M., 2001. Late 18th century drought-induced sand dune activity, Great Sand Hills, Saskatchewan. Can. J. Earth Sci. 38, 105–117.
Wolfe, S.A., Huntley, D.J., Ollerhead, J., 2004. Relict late Wisconsinan dune fields of the northern Great Plains, Canada. Géogr. Phys. Quatern. 58, 323–336.
Wolfe, S.A., Ollerhead, J., Huntley, D.J., Lian, O.B., 2006. Holocene dune activity and environmental change in the praire parkland and boreal forest, central Saskatchewan, Canada. Holocene 16, 17–29.
Zhen-shan, L., Xiao-hu, Z., Wen, H., 2008. A stochastic model for initial movement of sand grains by wind. Earth Surf. Processes Landforms 33, 1796–1803.
Zobeck, T.M., Van Pelt, R.S., 2006. Wind-induced dust generation and transport mechanisms on a bare agricultural field. J. Hazard. Mater. 132, 26–38.